



Filtration improvement and structure optimization of baffle promoter for tubular membrane

Jianxin Liu^{a,b,*}, Zhijun Liu^b, Fengxia Liu^b, Wei Wei^b, Xin Zhang^b

^aState Key Laboratory of Heavy Oil Processing, China University of Petroleum-Beijing, Beijing 102249, China, Tel./Fax: +86 010 89739050, email: liu.jiessie@gmail.com

^bFaculty of Chemical and Environmental and Biological Engineering, Dalian University of Technology, Dalian 116012, China, emails: 542978595@qq.com (Z. Liu), 314659345@qq.com (F. Liu), 2986164632@qq.com (W. Wei), xiaozhu.77@163.com (X. Zhang)

Received 23 January 2017; Accepted 15 July 2017

ABSTRACT

Baffle promoter is commonly used structure to reduce fouling and increase flux in tubular membrane filtration. Its function is attributed to the hydrodynamic enhancement for the flow field. The arrangement and size are important structure parameters that influence the performance of baffle promoter. In this paper, filtration improvement performance of baffle promoter was experimentally studied considering two arrangement parameters including phase angle and fan angle, as well as two size parameters including radius and space. Flow fields in the tubular membranes with corresponding baffle promoters were analyzed by computational fluid dynamics (CFD) method. The results showed that baffle arrangement type determined the eddy direction in the tubular membrane module, which accounts for the scouring effect for the particle deposition. Baffle structure sizes influenced the eddy shape and size between the baffles, which accounts for the local shear and turbulence intensity on the membrane surface. Within the scope of this study, baffle promoter with phase angle of 90°, fan angle of 180°, radius of 20 mm and dimensionless space of 2.50 obtained relatively high filtration improvement and low pressure drop, which was also consistent with the CFD result. This study can be useful for the optimal design of baffle promoter in tubular membrane filtration.

Keywords: Tubular membrane; Filtration enhancement; Baffle promoter; Computational fluid dynamics

1. Introduction

Membrane filtration has broad applications in wastewater treatment and purification areas due to its distinctive advantages such as high separation efficiency, little reagent addition and low energy cost compared with other separation methods [1–4]. However, membrane filtration performance was usually deteriorated by fouling, which mainly arises from the deposition of particles or the concentration of dissolved matters on the membrane surface [5–8].

Even though membrane fouling is inevitable, its negative effects can be alleviated through appropriate methods [9–12]. Previous investigations have shown that the formation and

development of fouling are related to the hydrodynamic condition on the membrane surface. Hydrodynamic enhancement by turbulence promoter is recognized as one effective way to control the membrane fouling [13,14].

Baffle promoter (or insert) is one type of turbulence promoters commonly used in tubular membrane filtration. Its function is analogous to the heat transfer effect of baffle plate in shell-and-tube heat exchanger. The alternative streams produced by the baffle result in large eddies on the membrane surface, so as to enhance the flow and mass transfer. Then, the fouling can be reduced and the filtration performance can be improved.

The filtration improvement mechanisms of baffle promoter have been researched by many scholars. Ahmad and Mariadas [15] installed several different types of helical baffle

* Corresponding author.

inserts in the tubular membrane module and investigated their flux enhancement for microfiltration. It was shown that the baffle insert reduce the hold-up of the feed and increase the flow velocity and wall shear rate in the membrane channel. Besides, secondary flow was produced and resulted in the flow instabilities in the vicinity of membrane. Combined with microfiltration experiment, the advantages of baffle promoter in fouling control and flux improvement were demonstrated. Popovic et al. [16] studied the effect of semi-elliptical blade baffle promoter on the intensification of microfiltration. Results showed that compared with the non-promoter situation, baffle promoter increased the permeate flux and reduced the energy consumption. Chiu and James [17] investigated the filtration enhancement of three different types of baffle promoters. The results showed that the alternating direction helical baffles achieved the greatest flux improvement, which was attributed to the flow configuration of the baffle produced. Jokic et al. [18] adopted response surface methodology approach to evaluate the effect of turbulence promoter on the permeate flux in the microfiltration of bakers' yeast suspension. Their results showed that suspension concentration was the most significant factor for the filtration without inserts, while TMP and feed flow rate were two more important factors for the filtration with inserts. Despite the flux improvement performance, turbulence promoter also results in the increase of pressure drop of the membrane module, which causes higher energy cost of filtration [19,20]. Therefore, the optimization of structure so as to effectively utilize the turbulence energy is also one of the important research issues for baffle promoter.

The understanding of the hydrodynamic enhancement mechanism is helpful for the design and development of baffle promoter. Computational fluid dynamics (CFD) method is commonly used tool to analyze the flow field in the membrane module with complex structures. Numerous studies on the flow field of membrane modules (includes flat sheet, spiral wound and tubular membranes modules) with different types of promoters have been performed. Ahmed et al. [13,21] investigated the influence of baffle position (on the concentric rod or on the wall) and feed flow direction on the flow field in the membrane module with CFD method. The authors concluded that the filtration enhancement of baffle promoter was ascribed to the wall velocity fluctuation and eddy generation in the flow field. Agreement between the experiment and simulation results also demonstrated the applicability of the CFD predictions. Popovic et al. [16,22] studied the flow field in the membrane modules with twisted tape, blade type baffle promoters, respectively, through CFD method. The results showed that baffle promoter changed the stream line and contributed to scouring effect for the deposited particles, which was favorable for the reduction of membrane fouling. Liu et al. [23,24] used FLUENT software to analyze the flow field in the tubular membrane module filled with circular baffle or helical screw insert. Their results showed that circular baffle produced eddies, while helical screw insert produced swirl flow around the tube axis. No stagnation flow zone occurred in the later flow field as the continuous structure of the screw insert with its energy cost lower than the other one. Jafarkhani et al. [25] established 3D simulation model to investigate the influence of structure parameters of semi-circular baffle involving pitch to baffle

diameter ratio and baffle orientation on the fluid dynamics in membrane tube. It was demonstrated that the flow and mass transfer on the tube wall can be enhanced with the increase of baffle angle. Monfared et al. [19] numerically studied the flow field in rectangular channels with six different arrangement baffles. By comparing the permeate flux results, the authors concluded that central baffling is arranged much better than the other five types. Previous investigations on the baffle promoter mainly focused on specific type or arrangement, while comprehensive evaluations of the influences of structure and size on the hydrodynamic enhancement as well as filtration performance are still necessary.

In this paper, experiments of diatomite suspension microfiltration were conducted on laboratory tubular membrane filtration platform. Baffle promoters with different structure parameters involving phase angle, fan angle, radius and space were inserted in the membrane module. The influences of every structure parameter on filtration improvement were tested. The flow field in the membrane module was obtained with 3D CFD simulation. The hydrodynamic enhancement mechanisms of baffle structure parameters were analyzed.

2. Membrane filtration experiment

2.1. Experimental setup

Fig. 1 is the tubular membrane filtration flow chart. In the experiment, the feed was pumped from the reservoir to the membrane module by centrifugal pump (CDL16, CNP Co., Ltd., China). The feed flow rate was adjusted through valve and lateral pipe line.

The inlet connected to the shell side was used for the filtration procedure, while the inlet connected to the tube side was used for the back-flushing procedure. Back pressure valve was set in the tube exit to adjust the transmembrane pressure (TMP). The permeate outflowed from the tube side to the permeate reservoir to measure the flux. The residual permeate returned to the feed reservoir to confirm the feed concentration constant. Pressure gauges P1, P2 and P3 were used to measure

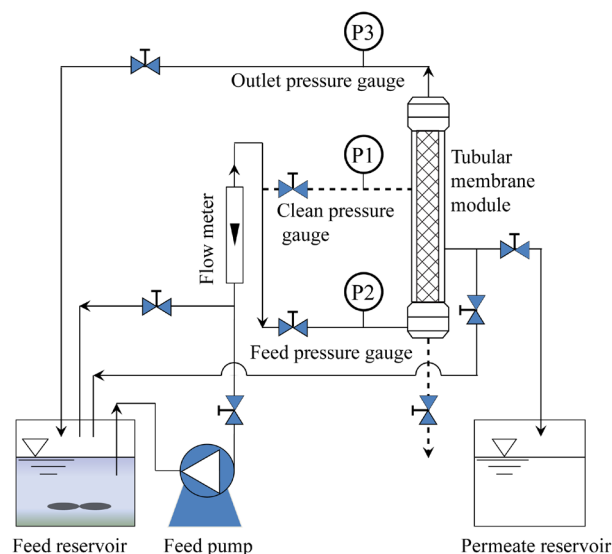


Fig. 1. Schematic of tubular membrane filtration experiment.

the pressure in the shell side inlet, tube side inlet and outlet, respectively. The feed flow rate was measured by rotameter.

Filtration procedure and backwashing procedure can be operated, respectively, by regulating the valves on both sides of the membrane module. In the filtration procedure, the inlet valve on the tube side was open and the valve on the shell side was closed. The feed entered the membrane module from the tube side and returned back to the feed reservoir after filtration. In the backwashing procedure, the feed was replaced with cleaning water. The inlet valve on the shell side was open, while the tube side valves and the permeate side valve were closed. The cleaning water entered from the shell side (as the dashed line). Fouling layer was removed from the membrane by the high pressure water jet and outflowed from the discharge valve.

Fig. 2 shows the structure of the membrane module. The membrane module was fabricated with polymethyl methacrylate (PMMA) and consisted of upper tube chamber, lower tube chamber and shell. Feed inlet and outlet were connected to upper tube chamber and lower tube chamber, respectively. Back-flushing inlet and outlet were connected to the shell. The tubular membrane was erected in the tube side and sealed with rubber bearing at the surface. Stainless core shaft was set in the membrane to install the baffle promoter. The ends of the core shaft were connected to the tube chamber flanges with screw bolts.

Fig. 3 is the tubular membrane filter cartridge used in the experiment. Polyester fiber membrane with a nominal pore size of 0.1 μm , length of 500 mm and diameter of 49 mm was inserted in the filter cartridge. The membrane was supported by non-woven fabric and stainless steel nets to prevent distortion caused by TMP.

The baffle promoter was fabricated with PMMA and was fixed in the membrane filter through one stainless steel core shaft. The structure of the baffle was shown in Fig. 4. In this paper, the influences of baffle radius r_d , baffle space l , fan angle β and phase angle α on filtration performance and flow field were investigated. Besides, in order to make the result more applicable, dimensionless baffle space $k_d = l/r_d$ was adopted.

2.2. Materials and methods

Diatomite suspension with a mass concentration of 1 g/L was used as the feed suspension. Particle size distribution



Fig. 3. Tubular membrane filter cartridge.

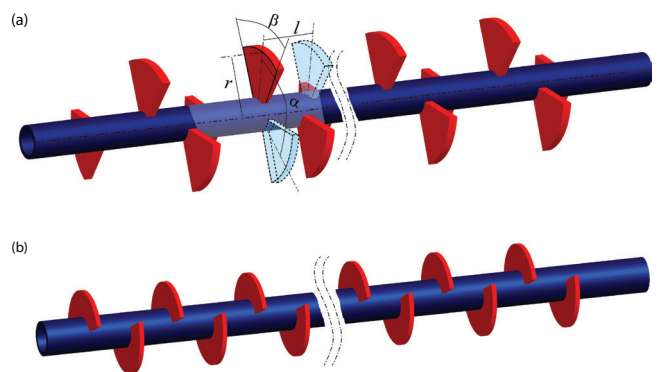


Fig. 4. Arrangement and structure of baffle turbulence promoters. (a) $\alpha = 60^\circ$, $\beta = 120^\circ$ and (b) $\alpha = 180^\circ$, $\beta = 90^\circ$.

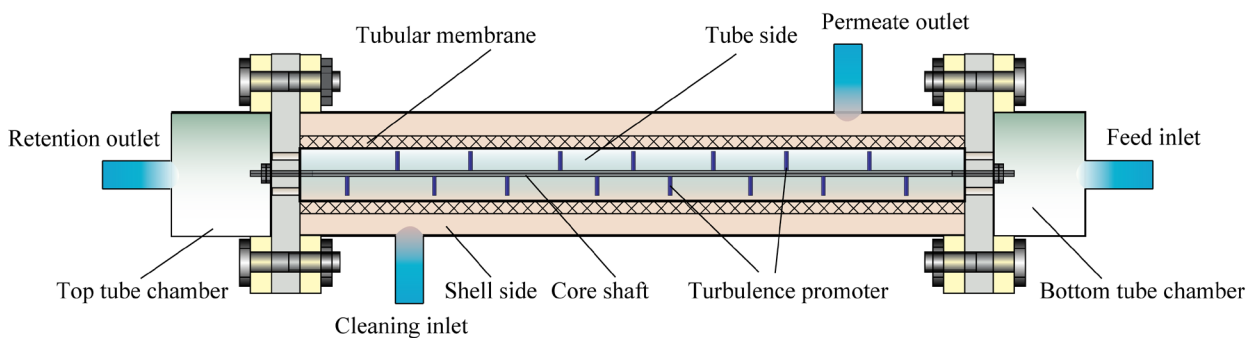


Fig. 2. Structure of tubular membrane filter.

was measured with laser particle size analyzer (BT-930, Better, China) and shown in Fig. 5. The minimum particle diameter was 4.14 μm, which was greater than the membrane pore size. This means that cake formation dominates the membrane fouling in the experiment.

During the filtration experiment, the permeate fluid was collected from the shell side to calculate the flux. As flux changed sharply in the initial filtration stage, the time interval for permeate collection was set as 2 min in the first 10 min. After then, the permeate fluid was collected every 5–20 min. The flux J was calculated with the following equation:

$$J = \frac{q}{A\Delta t} \quad (1)$$

where q is the permeate fluid volume; A is the effective membrane area; and Δt is the time interval. During the filtration process, the diatomite particle deposited on the membrane surface to form membrane fouling, which contributed to the increase of filtration resistance and the decrease of flux. However, when the flux attained certain value, the drag force arising from the permeate flow was equal to the lift force arising from the cross-flow. Then, particles stopped depositing and the flux achieved steady value. Higher steady flux can denote better performance of baffle for the filtration. In other word, the investigation of steady flux was helpful for the evaluation of the filtration improvement of baffle. Therefore, in this paper, long-term filtration was performed to ensure steady flux was attained.

The TMP and the pressure drop ΔP were calculated as follows:

$$\text{TMP} = \frac{P2 + P3}{2} \quad (2)$$

$$\Delta P = P3 - P2 \quad (3)$$

where $P2$ and $P3$ are the pressures at the feed inlet and retention outlet of the membrane module, respectively.

After every filtration procedure, the membrane module was backwashed completely to remove the fouling. Next, filtration experiment was conducted after the calibration of membrane performance with clear water.

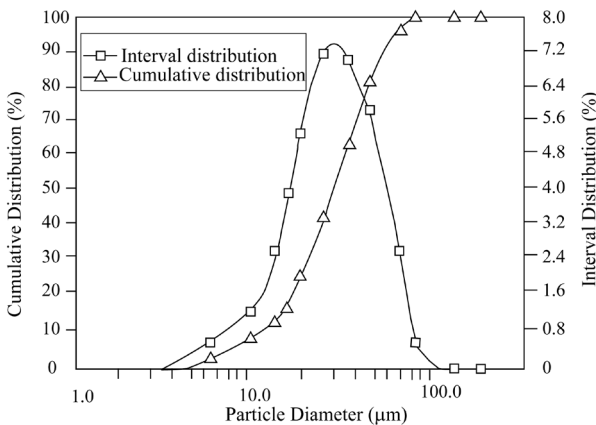


Fig. 5. Particle size distribution of diatomite.

2.3. Experimental results and discussion

As this study focus on the influence of baffle structure on filtration performance, all the experiments were performed under the same operation condition, that is, the TMP of 40 kPa and the feed flow rate of 4 m³/h.

2.3.1. The influence of baffle arrangement on filtration performance

The arrangement of the baffle affects the filtration enhancement performance of the baffle promoter. In this study, baffle fan angle represents the baffle arrangement type on the same axial position, while phase angle represents the twist of baffle group.

The twist of baffle on the core shaft had periodic feature, therefore, the phase angle was less than or equal to 180°. In this paper, four baffles with the same fan angle of $\beta = 180^\circ$, radius of $r_d = 18$ mm and space of $k_d = 2.5$ but different phase angles of 45°, 60°, 90° and 180°, respectively, were adopted to conduct the filtration experiment.

Fig. 6 shows influence of baffle phase angle on flux variation. The flux changes sharply in the early filtration stage and changes slowly in the following steady stage. In order the clearly shows the difference of flux variation under different conditions, these curves are depicted depending on two time subsections. In the early filtration stage, flux in four membrane

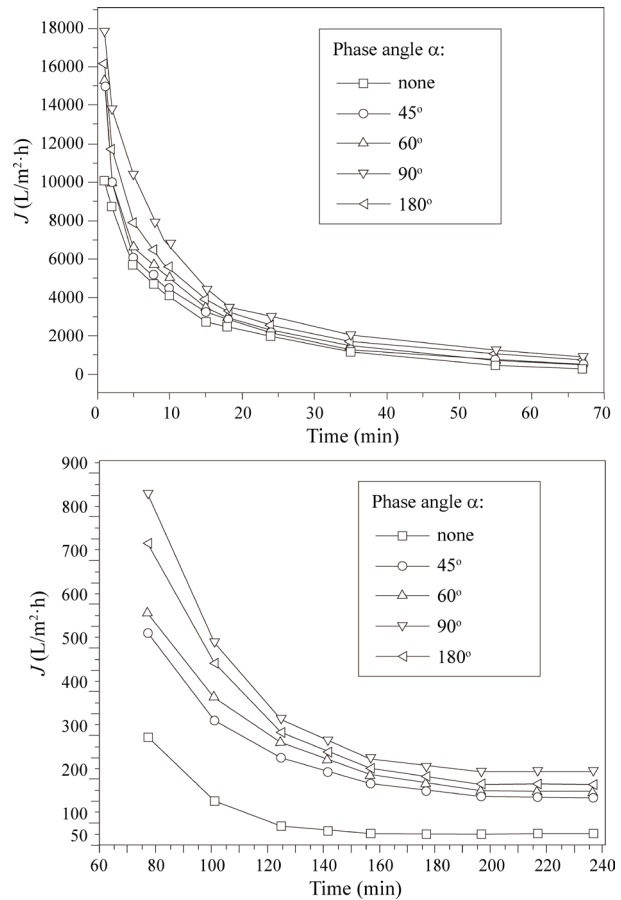


Fig. 6. The influence of baffle phase angle on filtration improvement.

modules decreases sharply, which is attributed to the rapid increase of membrane resistance. During the former 67 min, baffle promoter with phase angle of 90° has the highest flux, while the flux for baffle promoters with phase angle of 45°, 60° and 180° changes little compared with that of without baffle. This means there is no significant flux improvement of baffle promoter in the early filtration stage. After 170 min, flux obtained with four baffle promoters attained the steady state and the flux difference between baffle promoter and none baffle promoter become evident. The flux at baffle phase angle of 90° is 2.58 times as high as that without the baffle.

Keeping the phase angle of 90°, the influence of baffle angle on flux variation was investigated and shown in Fig. 7. It can be seen that the flux have the similar variation tendency and flux in baffle promoters with different fan angles were higher than that of without baffle. Baffle promoter with fan angle of 180° has the greatest flux improvement and the steady flux was 218.48 L/m² h, which was 2.91 times higher than that of without baffle. The steady flux at fan angles of 45° and 60° were similar, with the later one is relatively higher. This demonstrates that the flux enhancement of baffle increases with fan angle.

2.3.2. The influence of baffle space on filtration performance

Keeping the phase angle of 90° and fan angle of 180°, experiments for three baffle promoters with space of 35, 50

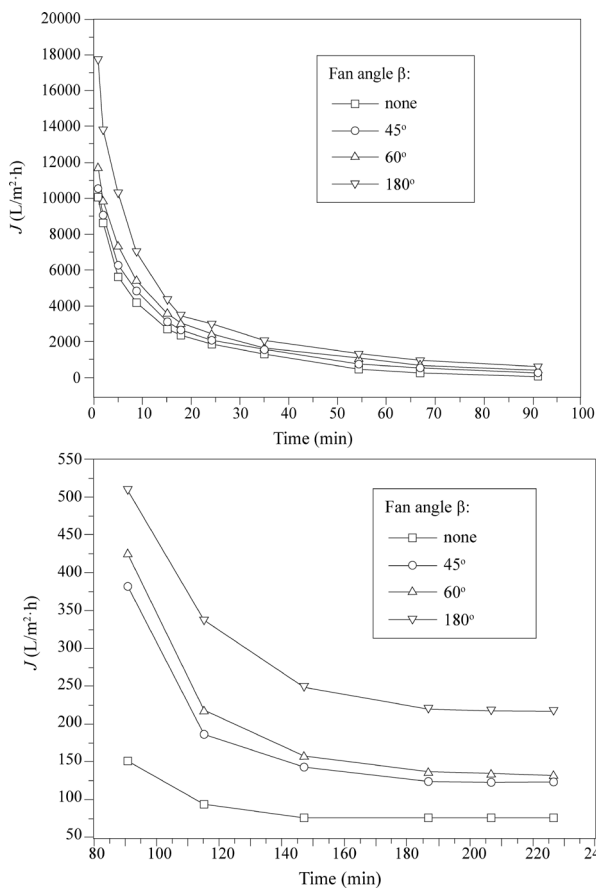


Fig. 7. The influence of baffle fan angle on filtration improvement.

and 65 mm, that is, dimensionless space k_d of 1.75, 2.50 and 3.25 were performed.

Fig. 8 is the flux variation for baffles with different spaces. It can be seen that in the early filtration stage, the flux decline sharply for none baffle membrane, while the flux decline slowly for baffles with different spaces. Baffle with $k_d = 2.5$ has the greatest steady flux, which is 3.24 times that of without baffle. The flux enhancement effect first increases and then decreases with the increase of baffle space.

2.3.3. The influence of baffle radius on filtration performance

Keeping $\beta = 180^\circ$, $\alpha = 90^\circ$ and $k_d = 2.5$, three baffles with radius of 18, 20 and 22 mm, respectively, were used in to test the influence of radius on filtration enhancement.

Fig. 9 was the influence of baffle radius on flux variation. It can be seen that in the early filtration stage, flux for $r_d = 22$ was higher, while for $r_d = 18$ mm or $r_d = 20$ mm, no obvious flux increase was shown compared with that of none baffle membrane. After 150 min, steady flux was obtained and the flux enhancement effect of baffle becomes evident. Besides, steady flux increases with the increase of baffle radius. For $r_d = 22$ mm, the steady flux was highest, which was 3.35 times that of none baffle membrane. This demonstrates that the flux enhancement effect increase with the increase of baffle radius.

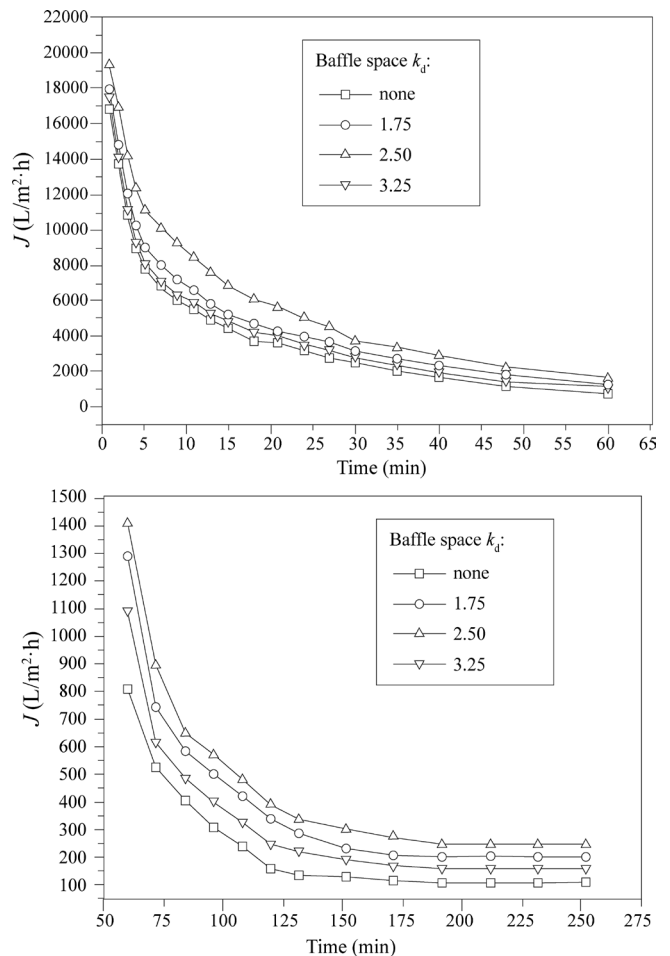


Fig. 8. The influence of baffle space on filtration improvement.

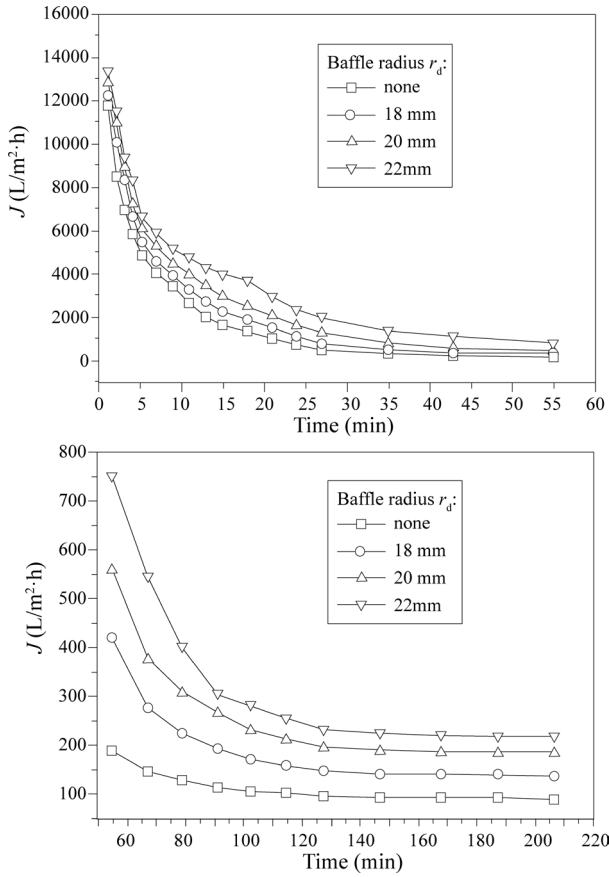


Fig. 9. The influence of baffle radius on filtration improvement.

3. Numerical study of the flow filed in the membrane module

3.1. Model development

As the obstacle of baffle, the fluid in the membrane module has a sinuous flow feature and the flow field was asymmetric. Besides, according to the experimental result, the average cross-flow velocity is higher than 0.6 m/s, while the permeate flow velocity is lower than 0.004 m/s. The influence of permeate flow on the cross-flow can be considered negligible. Therefore, a 3D simulation model was established based on the assumptions as follow:

- The feed was treated as single phase, continuous and incompressible fluid.
- The fluid was isotropic. Its property was independent on flow direction.
- The influence of permeation on flow field was neglected.

Turbulence flow velocity was the superposition of time-averaged flow and fluctuating flow. For incompressible flow, the continuity equations for these two flows are as follow:

$$\begin{cases} \frac{\partial u_i}{\partial x_i} = 0 \\ \frac{\partial u'_i}{\partial x_i} = 0 \end{cases} \quad (4)$$

where u_i and u'_i are the time average velocity and fluctuating velocity in the i ($i = x, y, z$) direction, respectively.

The momentum equation is the time-averaged Navier–Stokes, that is, Reynolds equation:

$$u_i \frac{\partial u_i}{\partial x_j} = -\frac{1}{\rho} \frac{\partial p}{\partial x} + \frac{1}{\rho} \frac{\partial}{\partial x_j} \left(\mu \frac{\partial u_i}{\partial x_j} - \overline{\rho u'_i u'_j} \right) \quad (5)$$

where $\overline{\rho u'_i u'_j}$ is the Reynolds stress term. As the Reynolds stress cannot be solved directly, turbulence model is incorporated to close the equations. Standard k – ε turbulence model, which has been proved to hold the advantages of high precision, good numerical stability and fast convergence, was used in this paper. In this turbulence model, turbulence energy k and dissipation rate ε , instead of the Reynolds stress, were solved with the following transport equations:

$$\begin{cases} \frac{\partial(\rho k)}{\partial t} + \frac{\partial(\rho k u_i)}{\partial x_i} = \frac{\partial}{\partial x_j} \left[\left(\mu + \frac{\mu_t}{\sigma_k} \right) \frac{\partial k}{\partial x_j} \right] + \mu_t \left(\frac{\partial u_i}{\partial x_j} + \frac{\partial u_j}{\partial x_i} \right) \frac{\partial u_i}{\partial x_j} - \rho \varepsilon \\ \frac{\partial(\rho \varepsilon)}{\partial t} + \frac{\partial(\rho \varepsilon u_i)}{\partial x_i} = \frac{\partial}{\partial x_j} \left[\left(\mu + \frac{\mu_t}{\sigma_\varepsilon} \right) \frac{\partial \varepsilon}{\partial x_j} \right] + \frac{C_{1\varepsilon} \varepsilon}{k} \mu_t \left(\frac{\partial u_i}{\partial x_j} + \frac{\partial u_j}{\partial x_i} \right) \times \frac{\partial u_i}{\partial x_j} \end{cases} \quad (6)$$

where the turbulence energy k and dissipation rate ε were written as follows:

$$\begin{cases} k = \frac{1}{2} \overline{u'_i u'_i} \\ \varepsilon = \frac{1}{2} \mu \overline{\frac{\partial u'_i}{\partial x_i} \frac{\partial u'_i}{\partial x_i}} \end{cases} \quad (7)$$

According to Boussinesq's eddy viscosity model, the Reynolds stress term was represented as follows:

$$\overline{u'_i u'_j} = \nu_t \left(\frac{\partial u_i}{\partial x_j} + \frac{\partial u_j}{\partial x_i} \right) - \frac{1}{3} \overline{u'_i u'_i} \delta_{ij} \quad (8)$$

where ν_t is the eddy viscosity and written as the function of k and ε .

$$\nu_t = C_\mu \frac{k^2}{\varepsilon} \quad (9)$$

Model constants were given as proposed by Launder and Spalding [26], where $C_\mu = 0.09$, $C_{1\varepsilon} = 1.44$, $\sigma_k = 1.0$, $\sigma_\varepsilon = 1.3$.

3.2. Mesh and boundary conditions

A 3D simulation domain with length of 494 mm and diameter of 49 mm, which was the same size as the tubular membrane module was formed. The baffles were adhered to a core tube and located in the center of the simulation domain. Fig. 10 shows the boundary conditions and mesh. The left side of the domain was set as velocity inlet boundary. The right side was set as pressure outlet boundary. Membrane and baffle surfaces were set as non-slip wall. 325,680 unstructured grids were used to mesh the simulation domain with

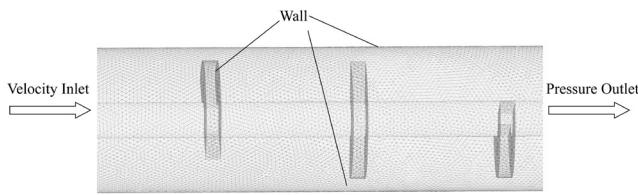


Fig. 10. Boundary conditions and mesh for the numerical simulation.

fine-grid treatment in the vicinity of the membrane surface. Based on the assumptions in section 3.1, water was used as the fluid in this simulation. The simulation was performed with FLUENT software, where pressure-based segregated method was used to solve the equations. The governing equations were discretized with second-order upwind method and SIMPLEC algorithm was applied for the velocity–pressure coupling. The numerical flow chart is illustrated in Fig. 11.

3.3. Numerical result and discussion

In order to reveal the hydrodynamic enhancement mechanism of baffle for tubular membrane filtration, numerical analysis of the flow field in the membrane modules were conducted. The influences of baffle phase angle, fan angle, baffle space and radius were studied.

Fig. 12 shows the flow fields in the membrane modules with three different fan angles. It is shown that the velocity significantly increases when the flow passing through the baffle, as the decrease of the cross-section area. With the cross-section area increase at the back of the baffle, the velocity then decreases while the pressure increase. Reverse pressure gradient was occurred at the back of the baffle, which drives the downstream fluid flow backward and produce eddy. The velocity in the eddy center is relatively lower while the velocity in the eddy periphery is high. Therefore, particles in the vicinity of the membrane can be entrained back into the eddy center, so as to mitigate the fouling. Besides, the repetitive obstacle for the flow results in significant velocity fluctuation, which intensifies the turbulence on the membrane surface and is favorable for the mixing of the fluid. In the flow fields of $\beta = 60^\circ$ and $\beta = 180^\circ$, the velocities in the area without baffle are higher than that with baffle. This demonstrates that the baffle enhances the flow at the opposite wall. It is also noted that even though the flow field distributes more homogeneous for $\beta = 45^\circ$, the velocity for $\beta = 45^\circ$ is relatively lower than the other two cases.

The local flow field distributions near the baffle for $\beta = 60^\circ$ and $\beta = 180^\circ$ were further compared and shown in Fig. 13. For $\beta = 60^\circ$, two low flow regions occurred under the baffle as the blue arrows designated. The surrounding fluid simply converged into these regions. For $\beta = 180^\circ$, anticlockwise spinning eddies occurred in the cross-section of the flow field. Along with the eddies in the longitudinal section of the flow field as shown in Fig. 12, spiral flow is produced in the membrane module, which is more beneficial for scouring the particles on the membrane surface.

The shear rate variation on the membrane surface for different phase angles and fan angles are shown in Fig. 14. As the baffles were repetitively arranged in the membrane

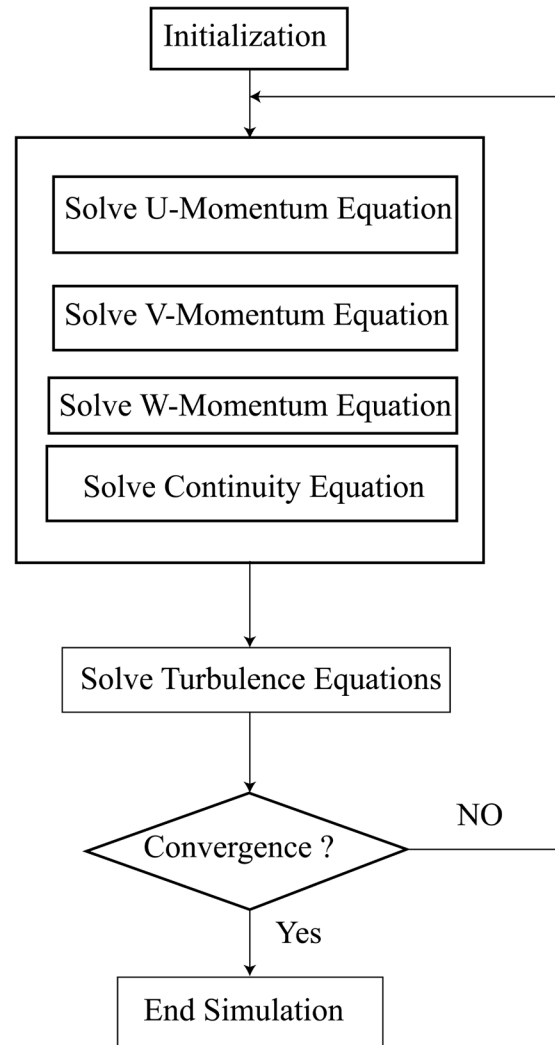


Fig. 11. Numerical flow chart.

module, the shear rate exhibited wave-like variation. The maximum shear rate occurs at the baffle position, while the minimum shear rate occurs between two adjacent baffles. Shear rate for baffle with $\beta = 180^\circ$ and $\alpha = 90^\circ$ is highest at the same position. Higher shear rate can enhance lift force of particle toward the main flow and is helpful for improving the filtration efficiency.

Besides the shear rate, baffle also enhanced the membrane turbulence as shown in Fig. 15. It can be seen that the turbulence energy for fan angle of 180° is higher than that for other two fan angles, while turbulence energy for phase angles of 60° and 90° are higher than that for other two-phase angles. The radial mixing of fluid on the membrane surface can be improved by turbulence, so as to reduce the particle deposition.

The flow field parameters for different fan angles and phase angles are listed in Tables 1 and 2. It is shown that the baffle with fan angle of 180° and phase angle of 90° exhibits the greatest membrane shear rate and turbulence energy. This can be attributed to the particular flow pattern in the

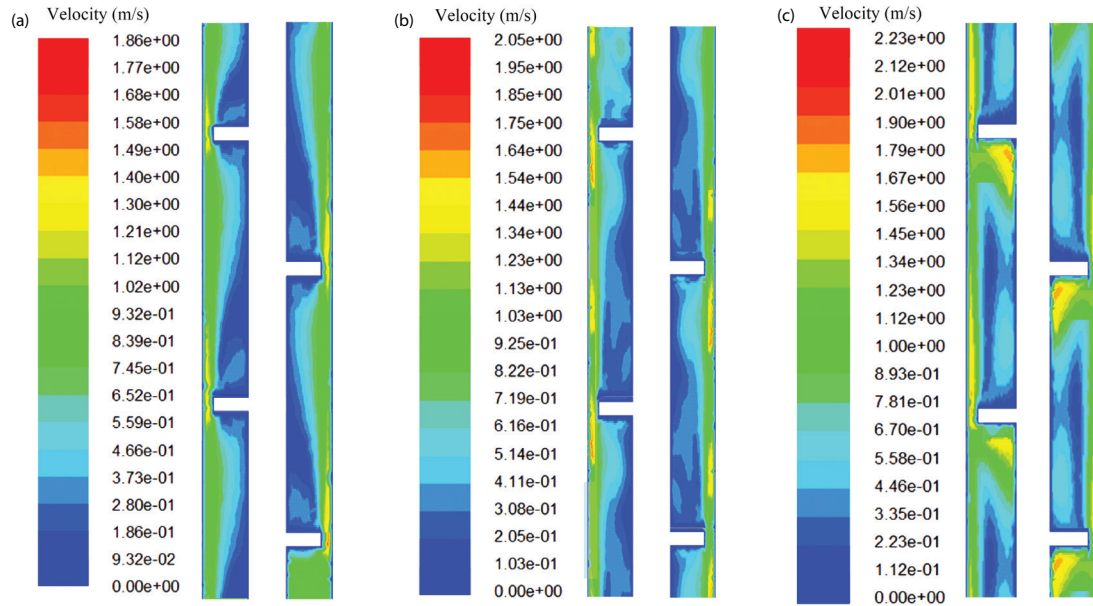


Fig. 12. The influence of baffle fan angle on flow field of membrane filter. (a) $\beta = 45^\circ$, (b) $\beta = 60^\circ$ and (c) $\beta = 180^\circ$.

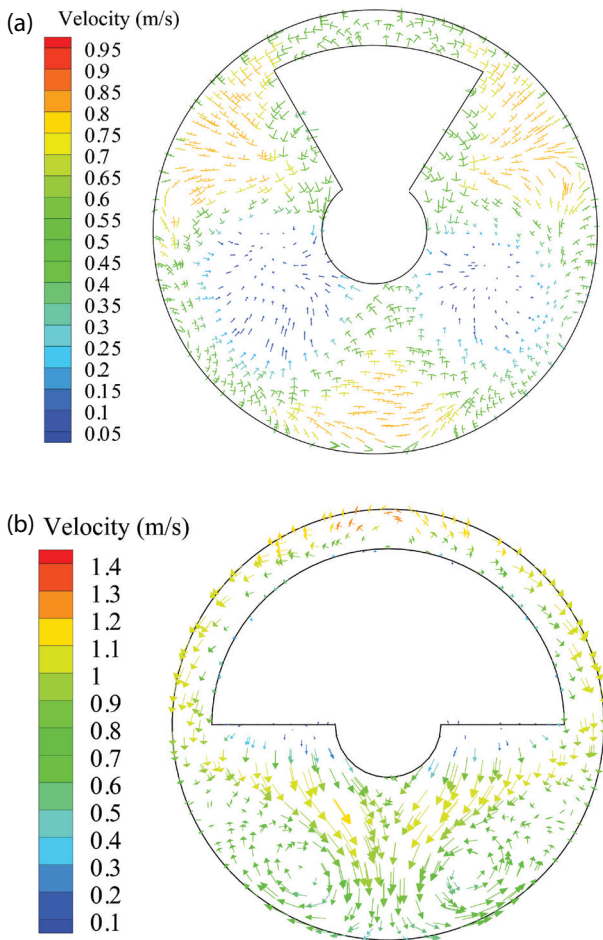


Fig. 13. Velocity vector distribution in cross-section of flow field. (a) $\beta = 60^\circ$ and (b) $\beta = 180^\circ$.

membrane module. The spiral flow produced by this type of baffle brings in double turbulence intensifications for the axial and radial flow. Therefore, the hydrodynamic condition as well as the filtration performance of membrane module is better improved. It should be noted that the negative influence of hydrodynamic intensification is the increase of pressure loss. The pressure drop for $\alpha = 90^\circ$ and $\beta = 180^\circ$ is more than 11 times as high as that for none baffle case. However, compared with the TMP, this pressure drop is negligible (only constitutes 5.2% of the TMP). Taking the evident filtration improvement performance into consideration, this type of baffle is fairly preferable.

Phase angle and fan angle influence the general flow pattern in the membrane channel, while the baffle space and radius influence the flow parameter distribution and strength between two adjacent baffles. Fig. 16 is the flow fields for three different baffle spaces. For all the three cases, eddies were observed at the back of the baffle, but the configuration and size of eddies were different. For $k_d = 1.75$, the eddy is small, with the reattachment point of eddy in the middle of two adjacent baffles. This indicates that the eddy has not been fully developed. The flow downstream from the reattachment point cannot be effectively enhanced. For $k_d = 3.25$, baffle space is long beyond the influence area of eddy, which is unfavorable for the transportation of particles downstream. Therefore, the particles entrained into eddy center would accumulate at the front of the baffle and result in serious local fouling. For $k_d = 2.50$, fully developed eddy generate homogeneous shear enhancement on the membrane surface. Fouling particles can be easily transported to the next baffle along with the periphery flow of eddy and eventually discharge from the membrane module. Therefore, the optimal baffle space should satisfy the full development of the eddy, while assuring the next baffle located at the periphery of the eddy.

The direct influence of baffle radius is the cross-section area of the membrane channel and result in the difference of

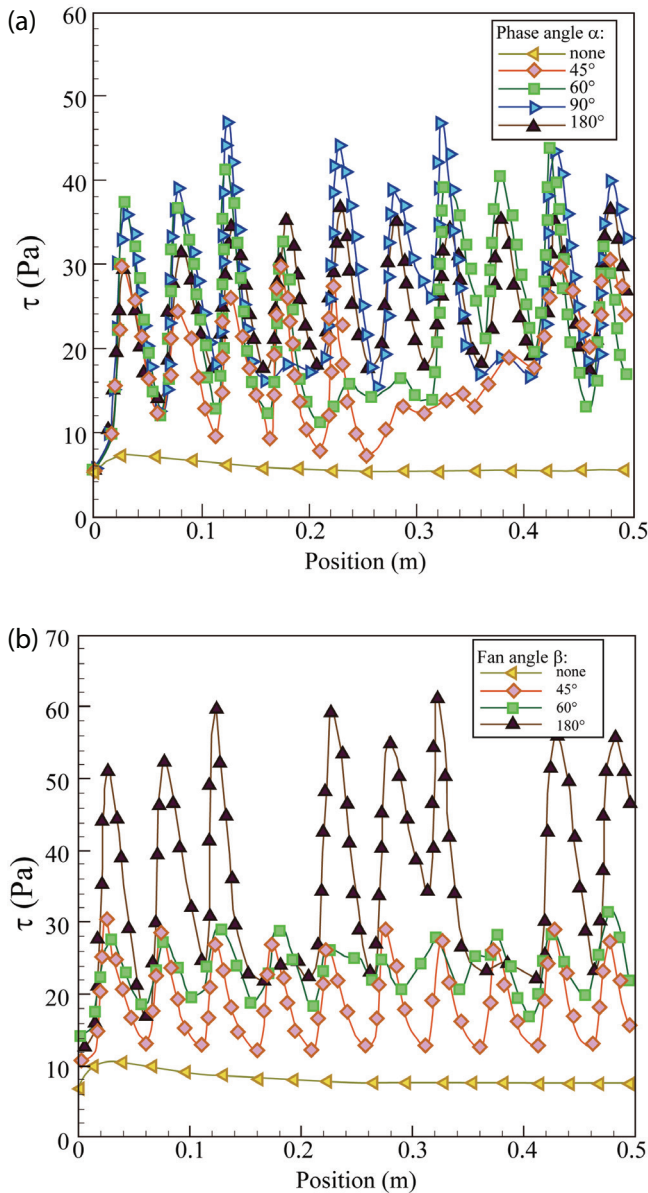


Fig. 14. Shear stress distribution under different baffle arrangements. (a) Influence of phase angle and (b) influence of fan angle.

membrane flow parameters. It can be seen from Table 3 that membrane shear rate and turbulent energy increase with the increase of baffle radius, which is favorable for the reduction of membrane fouling. However, even slight increase of baffle radius could result in significant increase of the pressure drop. The pressure drop for $r_d = 22$ mm is 7.3 times as high as that for $r_d = 18$ mm, which is far beyond the flux enhancement and uneconomical from the energy-saving point of view.

4. Conclusions

The influences of baffle promoter structure on filtration enhancement performance were tested by experiment. The hydrodynamic intensification mechanism of baffle promoter was analyzed with CFD method. The results showed that the arrangement type determine the general flow pattern in the

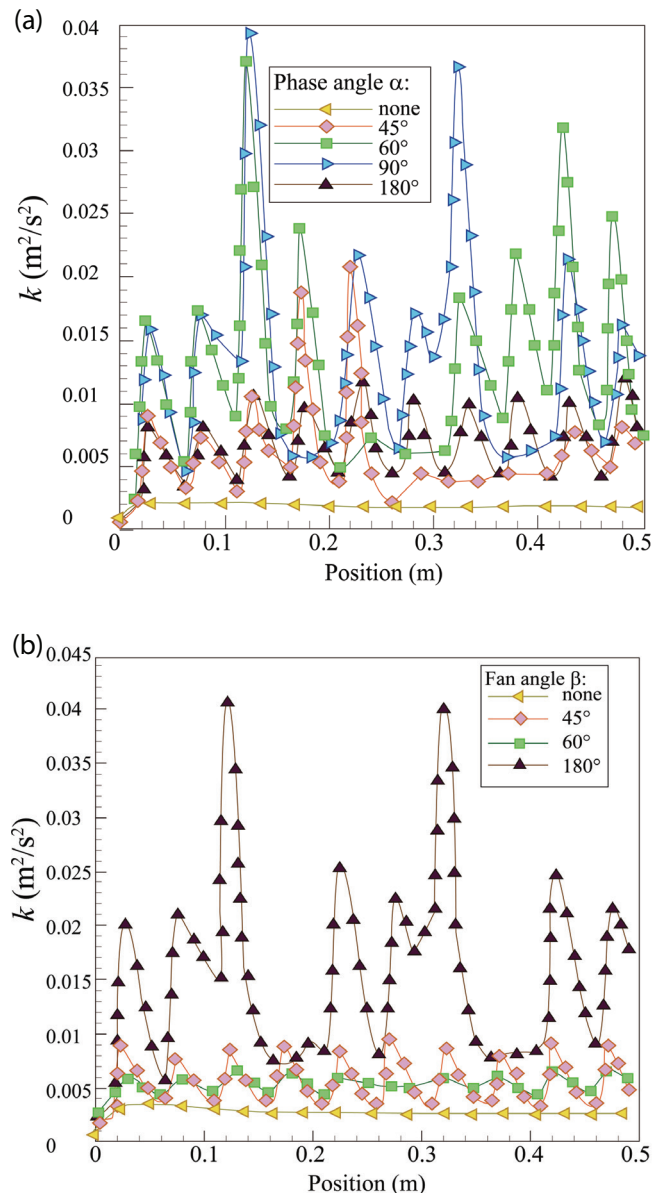


Fig. 15. Turbulence kinetic energy distribution under different baffle arrangements. (a) Influence of phase angle and (b) influence of fan angle.

Table 1
The influence of baffle phase angel on the flow field parameters

α	None	45°	60°	90°	180°
τ (Pa)	5.15	19.04	20.41	24.26	21.08
k (m ² /s ²)	0.002	0.007	0.013	0.025	0.009
ΔP (Pa)	175	1,214	1,479	2,072	1,684

membrane module, where phase angle influences the flow development along the axial direction, fan angle influences the velocity distribution in the cross-section. Within the scope of this study, baffle promoter with phase angle of 90° and fan angle of 180° produced highest shear the turbulence in the

Table 2
The influence of baffle fan angle on the flow field parameters

β	45°	60°	180°
τ (Pa)	19.45	21.35	24.26
k (m ² /s ²)	0.017	0.021	0.025
ΔP (Pa)	1,114	1,563	2,072

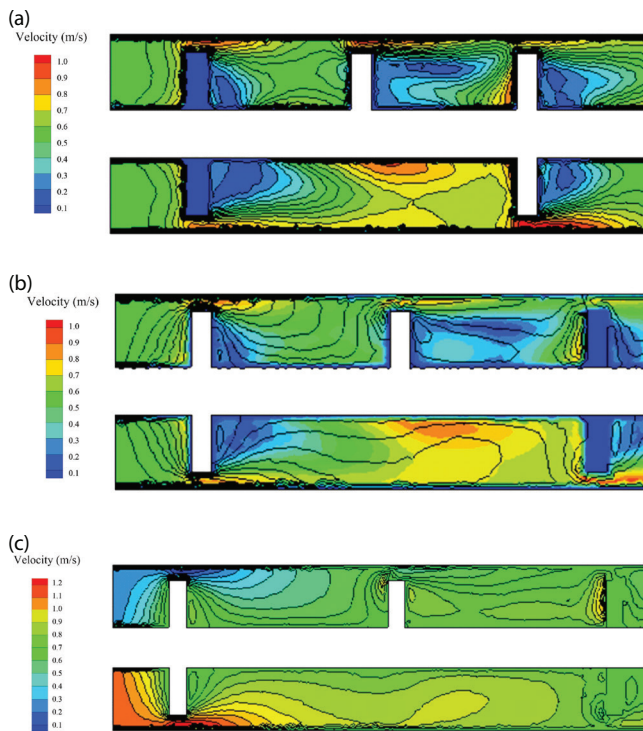


Fig. 16. The influence of baffle spacing on flow field of membrane filter. (a) $k_d = 1.75$, (b) $k_d = 2.50$ and (c) $k_d = 3.25$.

Table 3
The influence of baffle radius on the flow field parameters

r_d (mm)	18	20	22
τ (Pa)	24.26	42.19	75.32
k (m ² /s ²)	0.025	0.081	0.13
ΔP (Pa)	2,072	5,165	14,216

flow field, which account for the better filtration enhancement performance. Baffle space affect the eddy shape and size between the baffles. The optimal space should satisfy the full development of the eddy and assure the next baffle located at the periphery of the eddy. Increasing the baffle radius can narrow down the gap between baffle and membrane. Therefore, the membrane shear and turbulence can be greatly increased. However, slight increase of baffle radius also brings in significant increase of the pressure drop, which is unfavorable for the energy-saving consideration.

Symbols

A	—	Effective membrane surface, m ²
J	—	Permeate flux, L/(m ² h)

q	—	Volume of collected permeate fluid, L
l	—	Baffle space, m
k	—	Turbulence kinetic energy, m ² /s ²
k_d	—	Dimensionless baffle space
r_d	—	Baffle radius, m
TMP	—	Transmembrane pressure, Pa
u_i	—	Time averaged velocity, m/s
u'_i	—	Fluctuating velocity, m/s
ΔP	—	Pressure drop, Pa
Δt	—	Time interval of collecting permeation, s
α	—	Baffle phase angel, °
β	—	Baffle fan angel, °
ε	—	Dissipation rate
τ	—	Fluid density, kg/m ³
v_i	—	Shear rate, 1/s
ν_i	—	eddy viscosity (Pa·s)

References

- [1] A.A. Alturki, N. Tadkaew, J.A. McDonald, S.J. Khan, W.E. Price, L.D. Nghiem, Combining MBR and NF/RO membrane filtration for the removal of trace organics in indirect potable water reuse applications, *J. Membr. Sci.*, 365 (2010) 206–215.
- [2] A.L. Zydney, Membrane technology for purification of therapeutic proteins, *Biotechnol. Bioeng.*, 103 (2009) 227–230.
- [3] A. Cassano, C. Conidi, L. Giorno, E. Drioli, Fractionation of olive mill wastewaters by membrane separation techniques, *J. Hazard. Mater.*, 248 (2013) 185–193.
- [4] R. Singh, Production of high-purity water by membrane processes, *Desal. Wat. Treat.*, 3 (2009) 99–110.
- [5] S. Shirazi, C.J. Lin, D. Chen, Inorganic fouling of pressure-driven membrane processes – a critical review, *Desalination*, 250 (2010) 236–248.
- [6] A. Al-Amoudi, R.W. Lovitt, Fouling strategies and the cleaning system of NF membranes and factors affecting cleaning efficiency, *J. Membr. Sci.*, 303 (2007) 6–28.
- [7] D.D. Sun, Y. Wu, Use of laminar flow water storage tank (LFWS) to mitigate the membrane fouling for reuse of wastewater from wafer processes, *Membr. Water Treat.*, 3 (2012) 221–230.
- [8] A. Gasmi, M. Heran, A. Hannachi, A. Grasmick, Fouling analysis and biomass distribution on a membrane bioreactor under low ratio COD/N, *Membr. Water Treat.*, 6 (2015) 263–276.
- [9] E.M. Van Wagner, A.C. Sagle, M.M. Sharma, Y.H. La, B.D. Freeman, Surface modification of commercial polyamide desalination membranes using poly(ethylene glycol) diglycidyl ether to enhance membrane fouling resistance, *J. Membr. Sci.*, 367 (2011) 273–287.
- [10] N. Hilal, O.O. Ogunbiyi, N.J. Miles, R. Nigmatullin, Methods employed for control of fouling in MF and UF membranes: a comprehensive review, *Sep. Sci. Technol.*, 40 (2005) 1957–2005.
- [11] H.-M. Yeh, C.-H. Li, C.-C. Lin, Effect of gradually varying baffled-ring distance on ultrafiltration in tubular membranes inserted concentrically with a ring rod, *Desal. Water Treat.*, 26 (2011) 236–242.
- [12] X. Yang, R. Wang, A.G. Fane, C.Y. Tang, I.G. Werten, Membrane module design and dynamic shear-induced techniques to enhance liquid separation by hollow fiber modules: a review, *Desal. Wat. Treat.*, 51 (2012) 3604–3627.
- [13] S. Ahmed, M.T. Seraji, J. Jahedi, M.A. Hashib, CFD simulation of turbulence promoters in a tubular membrane channel, *Desalination*, 276 (2011) 191–198.
- [14] H.G. Goma, S. Rao, M. Al Taweel, Flux enhancement using oscillatory motion and turbulence promoters, *J. Membr. Sci.*, 381 (2011) 64–73.
- [15] A. Ahmad, A. Mariadas, Baffled microfiltration membrane and its fouling control for feed water of desalination, *Desalination*, 168 (2004) 223–230.

- [16] S. Popovic, D. Jovicevic, M. Muhadinovic, S. Milanovic, M.N. Tekic, Intensification of microfiltration using a blade-type turbulence promoter, *J. Membr. Sci.*, 425–426 (2013) 113–120.
- [17] T.Y. Chiu, A.E. James, Effects of axial baffles in non-circular multi-channel ceramic membranes using organic feed, *Sep. Purif. Technol.*, 51 (2006) 233–239.
- [18] A. Jokic, Z. Zavargo, Z. Seres, M. Tekic, The effect of turbulence promoter on cross-flow microfiltration of yeast suspensions: a response surface methodology approach, *J. Membr. Sci.*, 350 (2010) 269–278.
- [19] M.A. Monfared, N. Kasiri, A. Salahi, T. Mohammadi, CFD simulation of baffles arrangement for gelatin-water ultrafiltration in rectangular channel, *Desalination*, 284 (2012) 288–296.
- [20] H.-M. Yeh, C.-D. Ho, C.-H. Li, Effects of ring number and baffled-ring distances on ultrafiltration in the tubular membrane inserted concentrically with a ring rod, *Membr. Water Treat.*, 3 (2012) 51–62.
- [21] S. Ahmed, M.T. Seraji, J. Jahedi, M.A. Hashib, Application of CFD for simulation of a baffled tubular membrane, *Chem. Eng. Res. Des.*, 90 (2012) 600–608.
- [22] S. Popovic, M.N. Tekic, Twisted tapes as turbulence promoters in the microfiltration of milk, *J. Membr. Sci.*, 384 (2011) 97–106.
- [23] Y. Liu, G. He, L. Ding, H. Dou, J. Ju, B. Li, Experimental and CFD studies on the performance of microfiltration enhanced by a turbulence promoter, *Chin. J. Chem. Eng.*, 20 (2012) 617–624.
- [24] Y.F. Liu, G.H. He, X.D. Liu, G.K. Xiao, B.J. Li, CFD simulations of turbulent flow in baffle-filled membrane tubes, *Sep. Purif. Technol.*, 67 (2009) 14–20.
- [25] M. Jafarkhani, M.K. Moraveji, R. Davarnejad, F. Moztarzadeh, M. Mozafari, Three-dimensional simulation of turbulent flow in a membrane tube filled with semi-circular baffles, *Desalination*, 294 (2012) 8–16.
- [26] B.E. Launder, D. Spalding, The numerical computation of turbulent flows, *Comput. Methods Appl. Mech. Eng.*, 3 (1974) 269–289.